Supplemental Information

Boosting Photocatalytic Hydrogen Evolution by Ultrafast Charge Transfer in a ZnS-CdS Z-Scheme Heterojunction with an Intercalated Co_9S_8 Layer

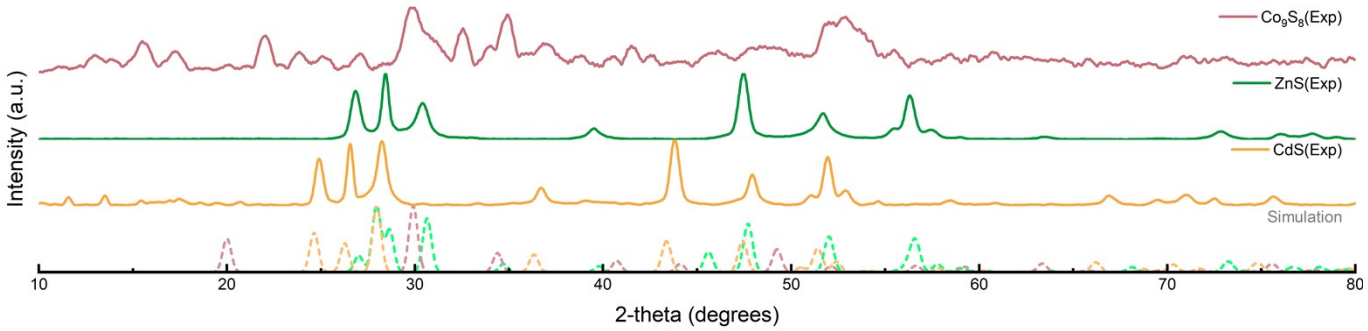

Supplementary Fig. S1. Crystallographic simulation and analyses: XRD analyse synthesized Co_9S_8, ZnS and CdS.

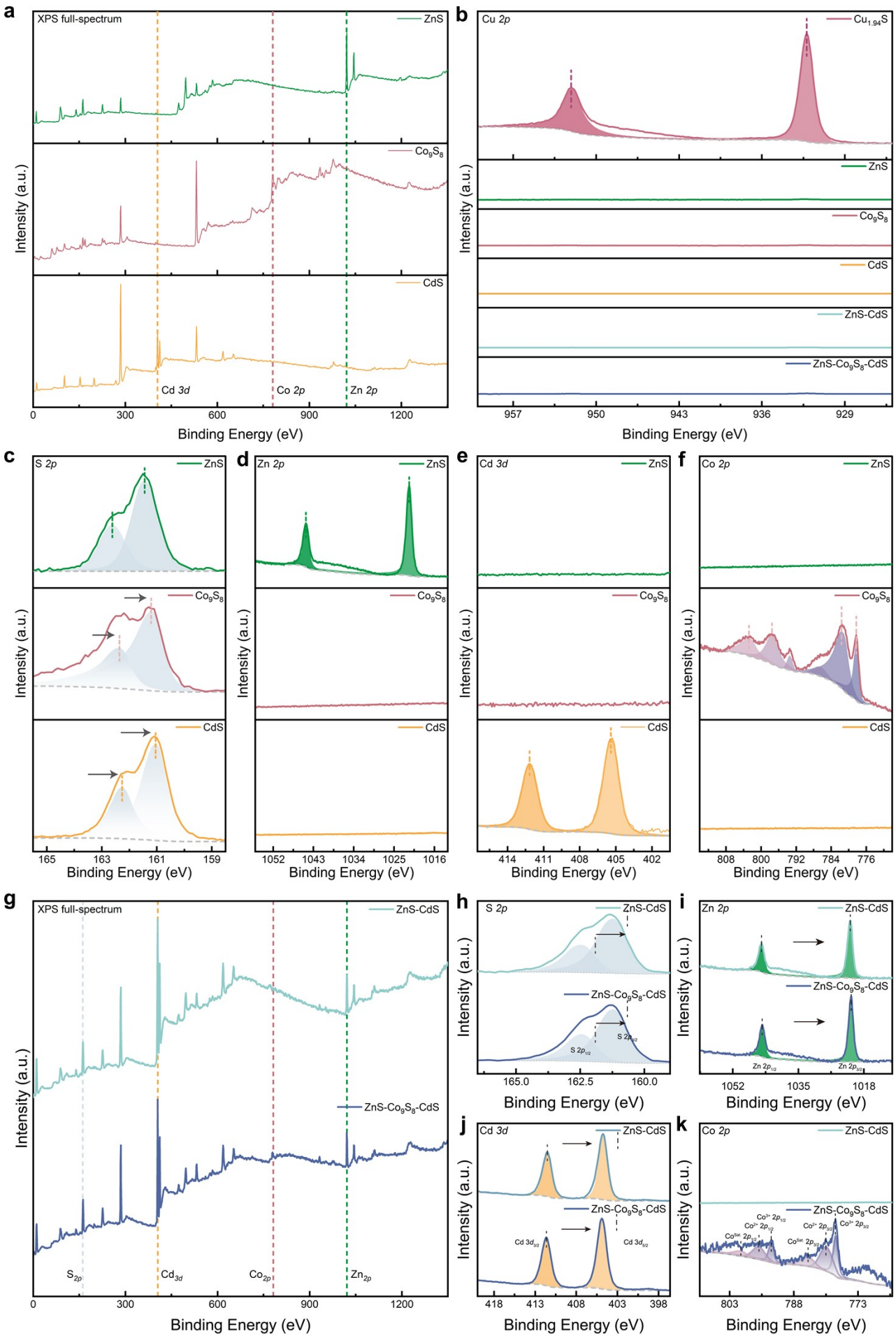

Supplementary Fig. S2. Chemical structure analysis: The XPS spectra of survey and high-resolution spectra of ZnS, Co9S8 CdS (a) full spectra (b) Cu *2p*, (c) S *2p*, (d) Zn *2p*, (e) Cd *3d*, and (f) Co *2p*. The XPS spectra of survey and high-resolution spectra of ZnS-CdS & ZnS-Co_9S_8-CdS (g) full spectra (h) S *2p*, (i) Zn *2p*, (j) Cd *3d* and (k) Co *2p*.

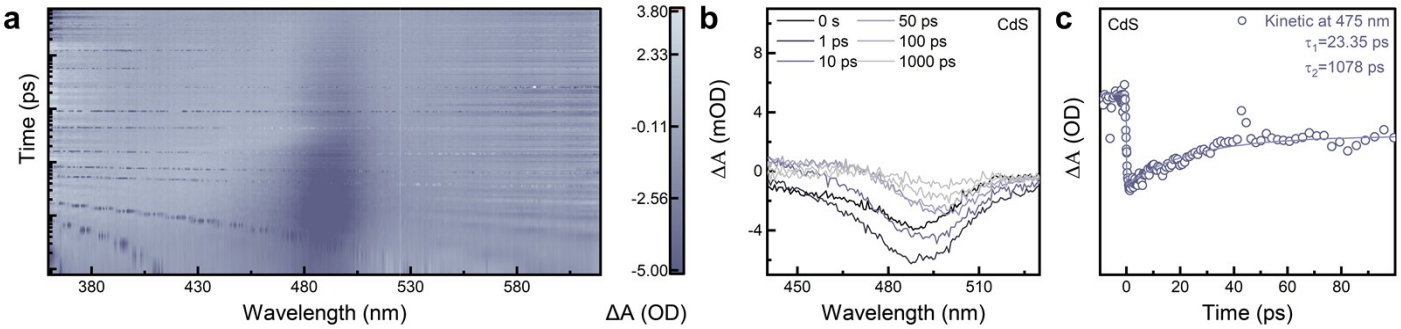

Supplementary Fig. S3. Photogenerated carrier dynamics analysis: (a) 2D pseudo colour fs-TA spectra for CdS. (b) fs-TA spectra of CdS. (c) Corresponding normalized fitted transient absorption kinetics of CdS probed at 325 nm with a delay time within 100 ps.

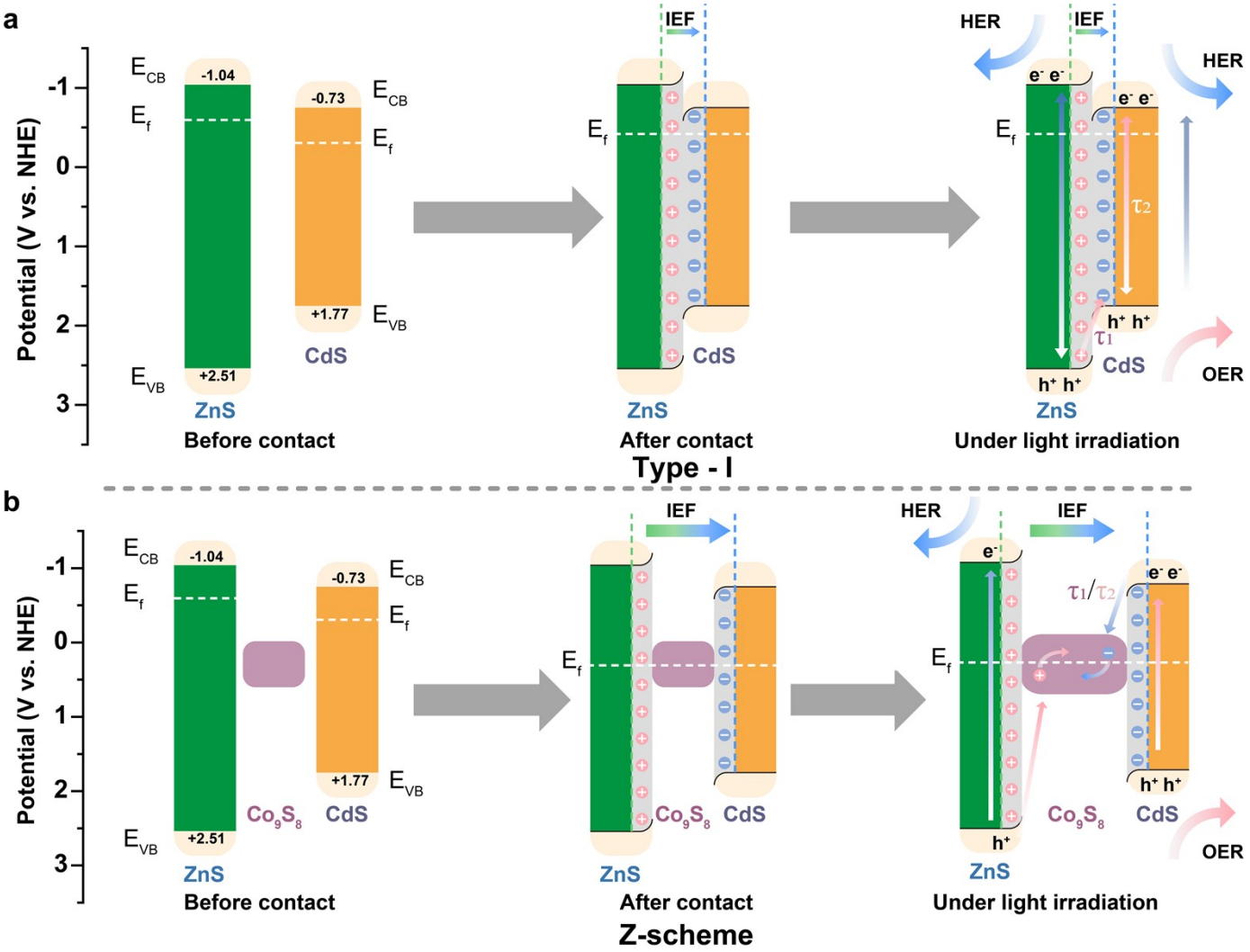

Supplementary Fig. S4. Band structure and charge carrier dynamics analysis: (a) Schematic illustration of the band structures of ZnS and CdS (left), interfacial charge transfer and the formation of an IEF upon hybridization (middle), and ZnS-CdS Type-I heterojunction under light irradiation (right). (b) Schematic illustration of the band structures of ZnS, Co_9S_8 and CdS (left), interfacial charge transfer and the formation of an IEF upon hybridization (middle), and ZnS-Co_9S_8-CdS Z-Scheme heterojunction under light irradiation (right).

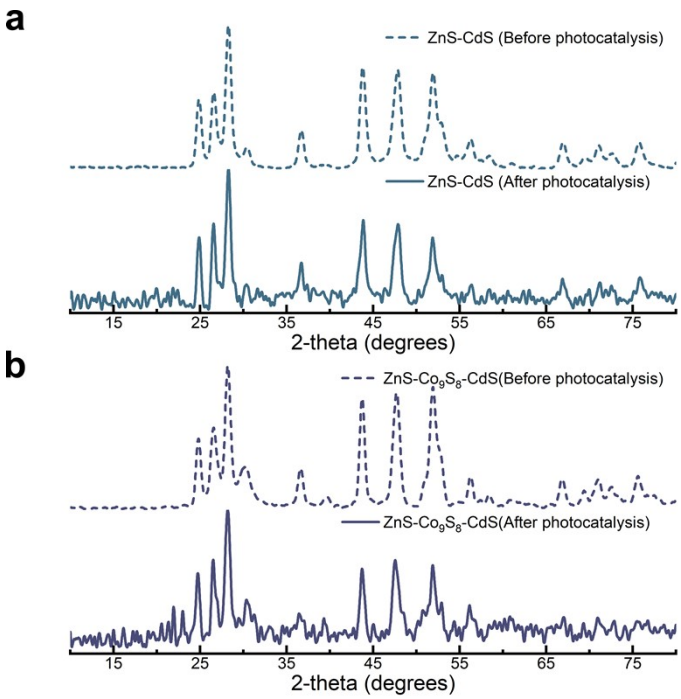

Supplementary Fig. S5 Photocatalyst durability analysis: XRD analysis of before and after photocatalysis for (a) ZnS-CdS and (b) ZnS-Co_9S_8-CdS.

2. Experiment

2.1 Materials

All chemicals were of analytical grade and used as received without further purification. Cadmium chloride ($CdCl_2$), copper (II) acetylacetonate ($Cu(acac)_2$), zinc chloride ($ZnCl_2$), and cobalt (II) chloride ($CoCl_2$) were purchased from Aladdin Scientific Corp. (Shanghai, China). Solvents including 1-octadecene (ODE), oleylamine (OLAm, 80-90%), and trioctylphosphine (TOP, 97%) were also obtained from Aladdin. Sodium sulphite (Na_2SO_3) and sodium sulphide nonahydrate ($Na_2S{\cdot}9H_2O$) were supplied by Sinopharm Chemical Reagent Co. Ltd.

2.2 Synthesis of $Cu_{1.94}S$ Rob

$Cu_{1.94}S$ nanorods were synthesized as the cation exchange template via a modified heating-up method [8]. Briefly, copper (II) acetylacetonate and trioctylphosphine oxide (TOPO) were dissolved in ODE under argon. After degassing, tert-dodecyl mercaptan (t-DDT) was injected at 80 °C, and the temperature was raised to 180 °C for 30 minutes. The resulting nanorods were purified by repeated centrifugation with hexane/ethanol mixtures.

2.3 Cation exchange reaction of ZnS, CdS, ZnS-CdS and ZnS-Co_9S_8-CdS

The ZnS-CdS and ZnS-Co_9S_8-CdS heterostructures were synthesized through a controlled sequential cation exchange process [9]. First, precursor solutions containing metal-oleylamine complexes (M^{2+} = Zn^{2+}, Co^{2+}, or Cd^{2+}) were prepared in ODE/OLAm mixtures at 200 °C under inert atmosphere.

For ZnS-CdS: A dispersion of $Cu_{1.94}S$ nanorods in TOP was injected into a hot solution containing a precise amount of Zn^{2+} precursor. After purification, the intermediate product underwent a second exchange with a Cd^{2+} precursor solution to yield the binary heterojunction.

For ZnS-Co_9S_8-CdS: The ternary heterostructure was achieved by a sequential three-step exchange. The template nanorods were reacted successively with Zn^{2+}, Co^{2+}, and finally Cd^{2+} precursor solutions. The molar ratio of the precursors was precisely controlled (e.g., 1/3 stoichiometry relative to the template for each cation) to achieve the targeted segmented architecture. Each exchange step was conducted at 120 °C for 30 minutes, with intermediate purification cycles.

Sample purification procedure: After synthesis, all products were isolated through addition of a 3:1 n-hexane:ethanol mixture, followed by subsequent centrifugation and resuspension in n-hexane. The centrifugation / resuspension process was repeated twice before the final product was suspended in n-hexane for characterization. The centrifugation set was 8500 rpm@5 min. Finally, the samples were dried under vacuum at 60 °C for 12 hours to obtain the final powder materials.

2.4 Structural and Optical Characterization

A suite of complementary analytical techniques was employed to investigate the morphology, crystallinity, and elemental composition of the synthesized $Cu_{1.94}S$ nanorods and their derivative heterostructures. Transmission electron microscopy (TEM) and high-resolution TEM (HRTEM) analyses were performed on an FEI Titan G2 60-300 field-emission microscope operating at an accelerating voltage of 300 kV. Elemental mapping was achieved via high-angle annular dark-field scanning TEM (HAADF-STEM) coupled with energy-dispersive X-ray spectroscopy (EDS), with the beam current carefully adjusted between 0.15 and 0.75 nA during acquisition. For TEM observations, samples were prepared by drop-casting a dilute dispersion of nanoparticles in n-hexane onto carbon-coated molybdenum grids. Phase identification was carried out by powder X-ray diffraction (XRD) using a Rigaku MiniFlex600 diffractometer with Cu Kα radiation (λ = 1.54 Å), scanning the 2θ range from 10° to 80°. Surface chemical states were probed by X-ray photoelectron spectroscopy (XPS) on a Thermo Scientific ESCALAB Xi^+ system equipped with a monochromatic Al Kα source; all binding energies were referenced to the adventitious carbon C 1s peak at 284.8 eV. Optical absorption properties across the ultraviolet-visible-near infrared (UV-vis-NIR) range were assessed in diffuse reflectance mode using a Shimadzu UV-1800 spectrophotometer.

2.5 Photoelectrochemical (PEC) Analysis

The photoelectrochemical behaviour, indicative of charge carrier dynamics, was evaluated using a standard three-electrode configuration connected to a Metrohm Autolab PGSTAT302N potentiostat integrated with a μStat-i 400 impedance analyser. Working electrodes were prepared by spin-coating an aqueous dispersion of the photocatalyst (1 mg mL^{-1}) onto fluorine-doped tin oxide (FTO) glass substrates, followed by annealing at 300 °C under a nitrogen atmosphere. The electrochemical cell consisted of the photocatalyst/FTO working electrode, a platinum foil counter electrode, and an Ag/AgCl reference electrode immersed in a 0.1 M Na_2SO_4 electrolyte solution. Transient photocurrent responses were measured under chopped illumination from a simulated solar source (AM 1.5G, 100 mW cm^{-2}) while applying a constant bias of 0.4 V versus Ag/AgCl. Electrochemical impedance spectroscopy (EIS) was conducted in the dark over a frequency range of 10^5 to 10^{-1} Hz with an AC amplitude of 10 mV. Mott-Schottky analysis was performed at a fixed frequency of 10^3 Hz under dark conditions to estimate the flat-band potential.

2.6 Assessment of Photocatalytic Hydrogen Evolution

Photocatalytic hydrogen production activity was quantified using a closed-gas circulation system (Labsolar-6A, Perfectlight) with online gas analysis performed by a gas chromatograph (GC 9790II, Fuli) equipped with a thermal conductivity detector. To enhance the hydrophilicity of the as-synthesized nanocrystals, a ligand exchange procedure was implemented: the catalyst was treated with formamide containing 3 vol% 3-mercaptopropionic acid (MPA) under sonication and subsequent stirring, followed by thorough washing with ethanol and deionized water. In a typical photocatalytic test, 10 mg of the surface-modified catalyst was dispersed in 100 mL of an aqueous solution containing 0.1 M Na_2SO_3 and 0.1 M $Na_2S{\cdot}9H_2O$ as sacrificial agents. The reactor was sealed, purged with argon to remove dissolved air, and the temperature was maintained at 10.0 ± 0.5 °C. The suspension was irradiated with simulated sunlight from a 300 W xenon lamp (PLS-SXE300D, Perfectlight) fitted with an AM 1.5G filter. Evolved hydrogen was monitored at regular intervals. Catalyst stability was evaluated through consecutive recycling experiments, wherein the system was evacuated and replenished with fresh sacrificial solution after each run without replacing the catalyst.

2.7 Femtosecond Transient Absorption measurements

Femtosecond transient absorption spectroscopy was utilized to probe ultrafast charge carrier dynamics. The experiments were conducted with a commercial Ti:sapphire regenerative amplifier system (Spectra-Physics Spitfire Ace) delivering 35 fs pulses at 800 nm with a 1 kHz repetition rate. A pump pulse at 325/650 nm was generated via optical parametric amplification, and its power was calibrated to 0.82 mW at the sample position. A white-light continuum probe beam (spanning 200–1600 nm) was produced by focusing a portion of the fundamental beam onto a translating sapphire crystal. Differential absorption (ΔA) signals were detected using a spectrometer (Andor SR-500i) synchronized with CMOS and InGaAs array detectors. The pump beam was focused on a spot size of approximately 100 μm on the sample cell. All measurements were performed on nanoparticle dispersions in n-hexane to minimize potential solvent interference.

Supplementary Table S1. Information of Chemicals used in synthesis and experiments.

Chemicals	CAS No.	Purity	Formula	Manufacturer	Cat. No.
Copper acetylacetonate	13395-16-9	≥97%	$Cu(acac)_2$	Aladdin Scientific Corp.	C109323
Zinc chloride	7646-85-7	≥98%	$ZnCl_2$	Aladdin Scientific Corp.	Z112526
Cobalt (II) chloride	7646-79-9	99.7%	$CoCl_2$	Aladdin Scientific Corp.	C106772
Cadmium chloride	10108-64-2	99.99%	$CdCl_2$	Aladdin Scientific Corp.	C116344
1-Octadecene	112-88-9	>90%	$C_{18}H_{36}$	Aladdin Scientific Corp.	O109487
Oleylamine	112-90-3	80-90%	$C_{18}H_{37}N$	Aladdin Scientific Corp.	O106967
Trioctylphosphine	4731-53-7	90%	$C_{24}H_{51}P$	Aladdin Scientific Corp.	T106625
Trioctylphosphine oxide	78-50-2	≥98%	$[CH_3(CH_2)_7]_3PO$	Aladdin Scientific Corp.	T106624
Tert-dodecanethiol	25103-58-6	98%	$C_{12}H_{26}S$	Aladdin Scientific Corp.	D106952
3-Mercaptopropionic acid	107-96-0	98%	$C_3H_6O_2S$	Aladdin Scientific Corp.	M103035
Formamide	75-12-7	99%	CH_3NO	Aladdin Scientific Corp.	F103361
Sodium sulphite	7757-83-7	98%	Na_2SO_3	Aladdin Scientific Corp.	S112300
Sodium sulphide nonahydrate	1313-84-4	≥98%	$Na_2S{\cdot}9H_2O$	Aladdin Scientific Corp.	S299093
Absolute ethanol	64-17-5	≥99.8%	CH_3CH_2OH	Sinopharm Chemical Reagent Co. Ltd.	10009259
Hexane	110-54-3	≥97.0%	$CH_3(CH_2)_4CH_3$	Sinopharm Chemical Reagent Co. Ltd.	800686191

Supplementary Table S2. XPS electron binding energies.

Sample	BE(eV)	Elements	Spectral Line
$Cu_{1.94}S$ NRs	161.5	S	$2p_{3/2}$
$Cu_{1.94}S$ NRs	162.6	S	$2p_{1/2}$
$Cu_{1.94}S$ NRs	932.4	Cu	$2p_{3/2}$
$Cu_{1.94}S$ NRs	952.3	Cu	$2p_{1/2}$
ZnS NRs	161.4	S	$2p_{3/2}$
ZnS NRs	162.7	S	$2p_{1/2}$
ZnS NRs	1021.6	Zn	$2p_{3/2}$
ZnS NRs	1044.7	Zn	$2p_{1/2}$
Co_9S_8 NRs	162.6	S	$2p_{3/2}$
Co_9S_8 NRs	163.9	S	$2p_{1/2}$
Co_9S_8 NRs	778.5	Co^{3+}	$2p_{3/2}$
Co_9S_8 NRs	793.6	Co^{3+}	$2p_{1/2}$
Co_9S_8 NRs	781.1	Co^{2+}	$2p_{3/2}$
Co_9S_8 NRs	797.2	Co^{2+}	$2p_{1/2}$
Co_9S_8 NRs	785.6	Co Satellite	$2p_{3/2}$
Co_9S_8 NRs	802.7	Co Satellite	$2p_{1/2}$
CdS NRs	405.4	Cd	$3d_{5/2}$
CdS NRs	412.2	Cd	$3d_{3/2}$
CdS NRs	161.1	S	$2p_{3/2}$
CdS NRs	162.3	S	$2p_{1/2}$
ZnS-CdS HNRs	161.2	S	$2p_{3/2}$
ZnS-CdS HNRs	162.5	S	$2p_{1/2}$
ZnS-CdS HNRs	1021.5	Zn	$2p_{3/2}$
ZnS-CdS HNRs	1044.6	Zn	$2p_{1/2}$
ZnS-CdS HNRs	404.8	Cd	$3d_{5/2}$
ZnS-CdS HNRs	411.5	Cd	$3d_{3/2}$
ZnS-Co_9S_8-CdS HNRs	161.2	S	$2p_{3/2}$
ZnS-Co_9S_8-CdS HNRs	162.5	S	$2p_{1/2}$
ZnS-Co_9S_8-CdS HNRs	1021.3	Zn	$2p_{3/2}$
ZnS-Co_9S_8-CdS HNRs	1044.4	Zn	$2p_{1/2}$
ZnS-Co_9S_8-CdS HNRs	404.9	Cd	$3d_{5/2}$
ZnS-Co_9S_8-CdS HNRs	411.6	Cd	$3d_{3/2}$
ZnS-Co_9S_8-CdS HNRs	778.3	Co^{3+}	$2p_{3/2}$
ZnS-Co_9S_8-CdS HNRs	793.3	Co^{3+}	$2p_{1/2}$
ZnS-Co_9S_8-CdS HNRs	780.6	Co^{2+}	$2p_{3/2}$
ZnS-Co_9S_8-CdS HNRs	796.3	Co^{2+}	$2p_{1/2}$
ZnS-Co_9S_8-CdS HNRs	784.9	Co Satellite	$2p_{3/2}$
ZnS-Co_9S_8-CdS HNRs	801.0	Co Satellite	$2p_{1/2}$

Supplementary Table S3. Fs-TAS fitting parameters.

Sample	τ_1(ps)	τ_2(ps)	A_1	A_2	Standard Deviation
CdS@325 nm	23.35	1078	-0.00325	-0.00107	0.000406
ZC@325 nm	16.46	775.1	-0.0159	-0.00662	0.00125
ZCC@325 nm	0.198	1.693	0.00515	-0.00319	0.000533
ZCC@650 nm	1.149	54.05	-0.05873	-0.1144	0.00453

$$A(t) = A1\exp\left(-\frac{t}{\tau 1}\right) + A2\exp\left(-\frac{t}{\tau 2}\right)$$

All fs-TAS signals were fitted using a double-exponential decay function:

τ_1 corresponds to the fast component (~1–10 ps), representing the initial ultrafast charge transfer process[11].

τ_2 corresponds to the slow component (10–1000 ps), reflecting recombination dynamics influenced by interfacial carrier separation or bulk defects recombination.

A1 and A2 are the amplitudes of the corresponding decay components.